# Investigation of zero/high field ion mobility orthogonal separation using a hyphenated DMA-FAIMS system and validation of the two-temperature theory at arbitrary field for tetraalkylammonium salts in nitrogen

Viraj D. Gandhi<sup>1,2,‡</sup>, Jihyeon Lee<sup>3,‡,†</sup>, Leyan Hua², Mohsen Latif², Christopher J. Hogan<sup>3,\*</sup>, Carlos Larriba-Andaluz<sup>2,\*</sup>

- <sup>1</sup> Department of Mechanical Engineering, Purdue University, 585 Purdue Mall, West Lafayette, IN 47907, United States
- <sup>2</sup> Department of Mechanical and Energy Engineering, IUPUI, 723 W. Michigan St., Indianapolis, IN, 46202, United States
- <sup>3</sup> Department of Mechanical Engineering, University of Minnesota, Minneapolis, MN, 55455, USA
- <sup>‡</sup> Shared co-first authorship. \*Corresponding co-authors: <u>clarriba@iupui.edu</u> / <u>hogan108@umn.edu</u>

ABSTRACT: Towards greater separation techniques for ions, we couple a differential mobility analyzer (DMA) with field asymmetric waveform ion mobility spectrometry (FAIMS) to take advantage of two mobility-related but differing methods in separation. The filtering effect of the DMA allows ions to be selected individually based on low-field mobility and studied in FAIMS at variable electric field, yielding mobility separations in two dimensions. Because spectra fully describe ion mobility at variable field strength, results are then compared with two-temperature theory-predicted mobility up to the fourth-order approximation. The comparison yields excellent results up to at least 100 Td, beyond which the theory fails to match the experiments. This is attributed to two effects, the enlargement of the structure due to ion heating and the inelasticity of the collisions with the nitrogen bath gas. The corrected mobility can then be used to predict the dispersion plot through a newly developed implicit equation that circumvents the possible issues related to the more elaborate Buryakov equation. Our results simultaneously show that the DMA-FAIMS coupling yields complete information on ion mobility versus field strength to gas density ratio, and works towards predicting such spectra from ion structures and gas properties.

Ion mobility spectrometry (IMS), in particular when coupled with the mass spectrometry (MS), is a state-ofthe-art technique for the separation and identification of compounds in the gas phase<sup>1-3</sup>. While IMS devices separate the ions based on their interaction potential with the buffer gas, MS systems distinguish them based on their mass, providing a quasi-orthogonal separation. For mobility separation, the ions are carried through a buffer gas using electric fields (E) <sup>4-6</sup>. The ions are assumed to instantly reach a drift velocity  $(v_d)$  which depends on the field and the ion's electrical mobility  $(K_h)$  through the equilibrium relation  $v_d = K_h E$ . The mobility is a somewhat complex function, with dependencies on the interaction potential between the ion and the gas, the size and mass of the ion, and the field over concentration  $E/n^{7,8}$ , also known as reduced field strength. Different devices exploit mobility dependencies in different ways to separate ions. Due to their differential selectivity, some IMS devices, such as differential mobility analyzers (DMA) and differential ion mobility spectrometry (DMS), can be

employed as a continuous supply of filtered ions to be fed into a mass spectrometer<sup>9-11</sup> with a clean background.

Such devices, however, do operate in very distinct manners. In a DMA<sup>12, 13</sup>, an electric field is applied between two parallel plate or concentric cylindrical electrodes and a gas with constant velocity is sheathed between them perpendicular to the field. A small slit is pierced in both electrodes offset by a distance L downstream on the bottom electrode as shown in figure 1a. Ions form mobility-based fan-shaped trajectories and only those with a specific mobility pass through the slit into the detector for a given field. The electric field can be scanned to produce a mobility spectrum. As they typically operate at atmospheric pressure, the reduced field strength is assumed low, and DMA devices normally rely on an assumed  $E/n \rightarrow 0$  mobility to separate ions.

DMS devices, on the contrary, separate ions based on the relative variation of the mobility with  $E/n^{14,15}$ , i.e. the normalized derivatives of the mobility with respect to the

field strength  $(1/K_0 \partial^p K/\partial E^p)$ , being p an integer. Here, in particular, we use high-field asymmetric waveform ion mobility spectrometry (FAIMS). In FAIMS, the ions flow into a parallel plate chamber using a carrier gas as shown in figure  $1b^{14, 16}$ . Inside, the ions are subjected to an asymmetric periodic electric field  $E_s(t)$  which is known as the separation field with period T.  $E_s(t)$  is characterized by a large difference in the electric field between the waveform's positive and negative polarities and is oriented perpendicularly to the gas flow. The waveform is specified

such that its periodic average is zero,  $\frac{1}{T}\int_0^T E_s(t)\,dt = \langle E_s(t)\rangle = 0$ , where the periodic averaging for any quantity is represented as  $\langle \ \ \rangle$ , and where the field satisfies  $\langle E_s^{2p+1}(t)\rangle \neq 0$  when  $p\geq 1$  <sup>17</sup>. One such example is a square wave in which  $E_s(t)$  is varied between  $E_{max}$  and  $E_{min}$  for time  $t_{max}$  and  $t_{min}$ , respectively. To satisfy the aforementioned conditions, the time period and the field are chosen such that

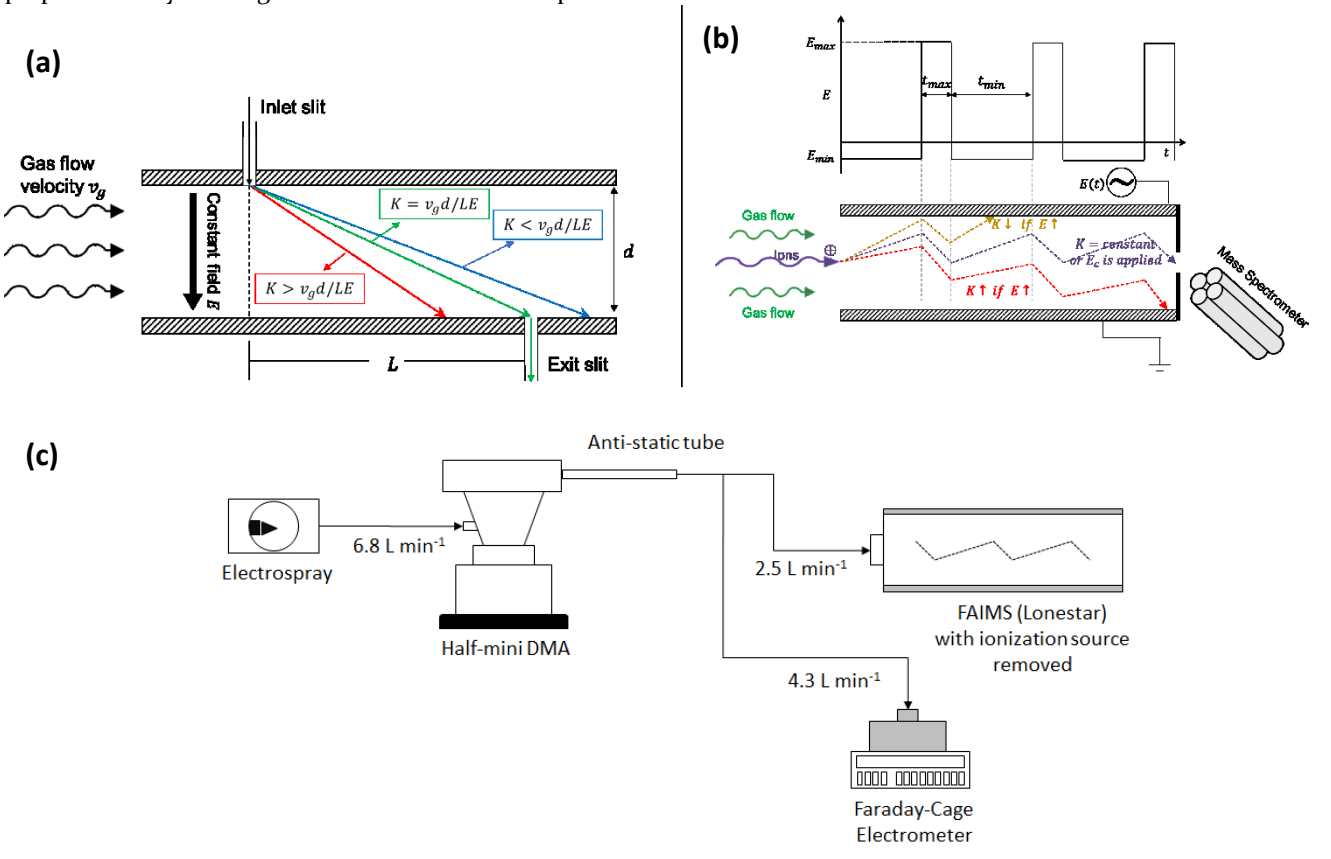


Figure 1.a) Schematic of a DMA device being used as a pre-filter to MS. Multiple ions enter through the inlet slit, however, only ions with a specific mobility can pass through the exit slit for a given electric field. The relaxation time in both velocity directions is negligible. Trajectory of various ions with decreasing order of mobility is showed in red, green, and blue colour respectively. b) Schematic of a FAIMS device being used as a pre-filter to MS. The motion of positively charged ions whose mobility increases, decreases, or stays unchanged by increasing electric field is illustrated using red, golden, and purple dashed lines respectively. The purple line also indicates the motion if the required  $E_c$  is provided. c) A schematic diagram of the electrospray-DMA-FAIMS tandem system utilized in the presented experiments, including transport flows.

 $E_{max}t_{max} + E_{min}t_{min} = 0$ . With the stated condition, if mobility was not a function of the field, all the ions would pass through the slit simultaneously. Different ions, however, experience a different net displacement in the vertical direction as a function of field strength<sup>2, 18-20</sup> depending on their behavior type as shown in Figure 2. To compensate for this displacement, an additional constant field or compensation field ( $E_c$ ) needs to be provided. Although all ions experience a total electric field  $E(t) = E_s(t) + E_c$ , filtering and high transmission can be attained.

While at first both devices, DMA and DMS/FAIMS, seem to provide a mobility measurement, as noted above, the two measurements are significantly different. The

work presented here examines the coupling of a DMA and FAIMS in series with N<sub>2</sub> as the drift gas. We show that this instrument combination enables determination of the field dependent mobilities of tetra-alkylammonium ions, and in doing so validating the advantages of coupling these orthogonal techniques to aid in the separation and identification process. Subsequently, with unique mobility versus E/N data (parameterized through known zero-field mobility FAIMS curves), we then verify two-temperature model predictions of field strength-dependent mobility in polyatomic gases, with calculations performed via IMoS <sup>21, 22</sup>. This brings an important level of quantification to non-linear mobility measurements, a topic of considerable recent interest<sup>23-30</sup>.

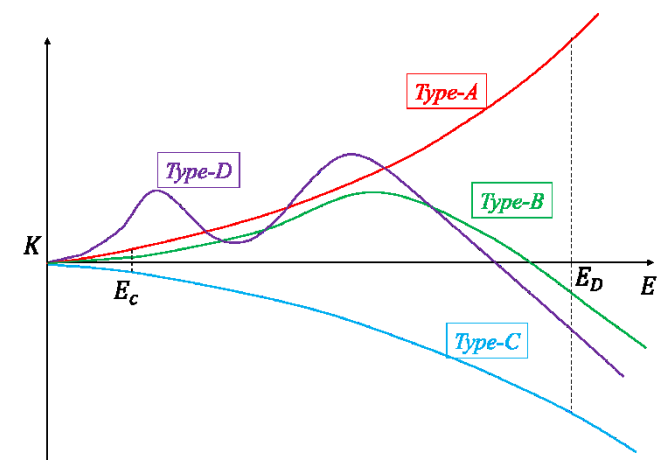


Figure 2. Mobility as a function of the field for different types of ions. The mobility of type-A ions increases with the field. The mobility of type-B ions increases and then decreases. The mobility of type-C ions decreases with increasing the field. The behavior of type-D ions varies with the field. This behavior is only observed at cryogenic temperatures and it is explained in ref<sup>21</sup>.

# Methods and Experimental setup

Tetrabutylammonium iodide (TBAI), tylammonium bromide (THAB), tetradecylammonium bromide (TDAB), and tetradodecylammonium bromide (TDDAB) were purchased from Sigma-Aldrich. 2mM of each sample was dissolved into methanol and introduced into a 1mL vial. The samples were ionized and sprayed into a commercially-manufactured half-mini DMA (Nanoengineering, Boca Raton, FL31) using electrospray ionization (ESI) as described in ref<sup>32, 33</sup>. A voltage of 2-3 kV was applied to the electrode inserted in the sample while a fused silica capillary tube with an inner diameter of 40µm was immersed in the vial. The sample vial was pressurized by a syringe to push the liquid through the capillary tube to other end located inside a chamber having inlet and outlet gas sampling ports. A filter and a diffusion drier were placed at the chamber intake, and the outflow was directly linked to the inlet of a half-mini DMA. The chamber included glass windows on both sides, to observe if a Taylor cone had developed. The current was measured and kept at 100-200 nA to preserve the stability of the electrospray through measurements. The DMA was operated with a circulating sheath flow of air by a vacuum blower. A heat exchanger was employed to keep the temperature of the sheath flowrate at room temperature by preventing it from being impacted by the blower. The design of the DMA is explained in 34 and reproduced in figure 1a for the reader. Through the geometry of DMA, it can be derived that the mobility of ion is given by:

$$K = Q_{sh} \frac{\ln\left(\frac{r_{out}}{r_{in}}\right)}{2\pi LV},\tag{1}$$

where  $Q_{sh}$  is sheath flowrate, L is length (20 mm), V is the voltage,  $r_{out}$  is the outer radius (6 mm), and  $r_{in}$  is the inner radius of the DMA (4 mm). The inner electrode of the DMA received a negative voltage through an external power supply, while the outer electrode was grounded.

The DMA output was split between an electrometer and FAIMS. The electrometer was used to detect the ion intensity coming out of the DMA while varying the electrode voltage for a given sheath flowrate. The mobility is then calculated using a reference calibrant, THA<sup>+</sup> <sup>35</sup>, to provide a quasi-zero field mobility.

With the DMA voltage held constant to select a known mobility, ions were continuously transmitted from the DMA outlet, through an antistatic tube 7.6 cm in length, similar to those describe by Attoui & Fernandez de la Mora for application in transmitting ions from DMAs<sup>36</sup>. Importantly the inner electrode of the DMA was the powered electrode, hence ions were transmitted by flow against an adversarial electric field through this tube, with non-negligible ion losses. Subsequently, the ion flow was split, going to both a Faraday cage electrometer and the FAIMS unit. The commercial FAIMS unit applied (Lonestar, Owlstone Inc, Westport, CT, USA) customarily samples neutral analytes at atmospheric pressure, using an Ni-63 source at its inlet for ionization. Following instructions provided by the manufacturer and under the supervision of University of Minnesota Department of Radiation Safety staff, this Ni-63 source was removed for coupling with the DMA, such that the FAIMS only sampled pre-ionized, mobility-filter analytes transmitted through the DMA. The FAIMS setup was used to investigate the mobility dependence of the identified peak tetraalkylammonium (TAA) ions on E/n. The parallel plate FAIMS used in this study is made using two 300 µm long plates spaced by  $d = 35 \mu m$ . The plates experience an asymmetric voltage with a frequency of 25MHz. Ions oscillate between the parallel plates under the influence of the field given by  $E(t) = E_c + E_s(t)$  where the separation field is characterized as  $E_s(t) = E_s \cdot f(t)$ , being f(t) the periodic waveform. For reasons described elsewhere<sup>37, 38</sup>, a bisinusoidal waveform was chosen as f(t) which can be defined as  $f(t) = \left(2\sin(\omega t) + \sin\left(2\omega t - \frac{\pi}{2}\right)\right)/3$ . The separation voltage  $(V_s = E_s d)$  was varied from 0 to 214 V in increments of 2%. At each separation voltage, the compensation voltage was swept from -6 V to 6 V with 512 steps. Ions with an average vertical velocity  $\langle V_c \rangle =$  $\langle K_h(E) \cdot E(t) \rangle = 0$  will be detected at the exit of FAIMS. The ion intensity is measured at a charge collector, biased at a negative 55 V. Finally, the intensity was then used to map a dispersion plot of  $E_c$  vs  $E_s$ . Each contour plot consists of 26,112 data points (512  $E_c$  by 51  $E_s$  values). The dispersion curve can provide a plethora of information, including how the relative mobility varies with the field. However, the zero-field mobility is not a direct value obtainable via FAIMS alone. A complete schematic diagram of the electrospray-DMA-FAIMS system is provided in figure 1c along with N<sub>2</sub> carrier gas flows. The entire system was operated at atmospheric pressure and room temperature, for all measurements.

#### Results and discussion

## **DMA & FAIMS Spectra**

Mobility spectra at a negligible electric field  $(K_0)$ , not to be confused with reduced mobility, were first measured using the electrospray-DMA-Electrometer path of the experimental system. The intensity was observed in the electrometer while the sheath flow rate in DMA was kept constant at 257 L/min (determined through calibration) at 1 atm pressure and 295K temperature, and the potential on the center rod was varied. Once the voltage that enables the highest transmission for that particular ion is known, the calibrant is used to determine the mobility. Figure S.1 displays the observed intensity vs inverse mobility. Ion mobilities for TBA+, THA+, TDA+, and TDDA+ were 1.42 cm<sup>2</sup>/Vs, 0.97 cm<sup>2</sup>/Vs, 0.78 cm<sup>2</sup>/Vs, and 0.72 cm<sup>2</sup>/Vs respectively which differ by less than 2% from the mobility observed by Ude and Fernandez de la Mora<sup>35</sup>. Along with monomer ions, dimer ions and doubly charged clusters were labeled in the figure where their mobilities, also reported by Ude and Fernandez de la Mora, allowed for their identification. Each ion concentration is on the order of 105/cm3 except for TBAI, which was 2x10<sup>4</sup>/cm<sup>3</sup>. We note that in preliminary experiments, we found this high concentration is necessary to ensure an adequate ion population for DMA-FAIMS experiments as there are considerable ion losses throughout the measurement system, notably at the DMA outlet where ions travel via flow against an adversarial electric field36 and at the inlet of the FAIMS, where losses of pre-ionized analyte due to both diffusion and to inlet electric fields were found significant. The applied DMA-FAIMS system was not optimized for ion transmission, which would likely require custom design of a DMA outlet -FAIMS inlet to optimize ion transmission (or possibly a FAIMS outlet-DMA inlet, as instrument order can be switched). For the present system, only a small percentage of the originally generated tetra-alkylammonium ions are ultimately transmitted through the DMA and FAIMS filters.

Two-dimensional FAIMS plots are provided for the monomer tetraalkylammonium ions in figure S.2, isolated from their multiply charged cluster ions using the DMA upstream. In this figure, for the 35  $\mu$ m gap between the plates and for 295K and 1atm of Nitrogen gas, 100% separation voltage corresponded to 245.8 Td. Unfortunately, the curve of TBAI fades at higher separation voltage since the ion transmission from DMA was deficient due to its higher zero-field mobility and diffusion coefficient. In figure 3 the centerlines of the dispersion curves are combined into a single plot to compare the compensation voltages for different ions. The figure shows that the compensation voltages for TDA and TDDA are similar for the whole range of separation voltages and thus to separate them in a mixture, it would be necessary to use DMA or low-field mobility spectrometer in tandem with FAIMS. In general, it can be observed that as the size of the ion increases, the required  $E_c$  for a given  $E_d$  decreases, indicating that the relative reduction in mobility of larger ions is less than that of small ions. However, the trend is reversed for TDDA and TDA. We presently have no explanation for this reversal which, given how close their variations are, might be caused by a small difference in pressure, temperature, the accuracy of the power supply, and the tolerance of distances, among others. The overall results displayed here however agree with the trend shown in <sup>39-41</sup> and confirm that the mobility of TAA ions decreases by increasing the electric field since higher compensation voltage in the same polarity is required at higher separation voltage.

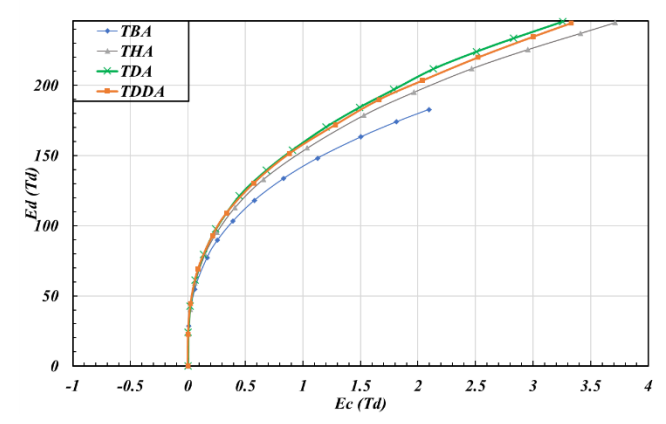


Figure 3. Extracted centerline from experimental dispersion curves in Figure S.2. The centerline of TDA and TDDA overlaps until 200Td and then slightly diverges.

#### Theory and Numerical Calculations

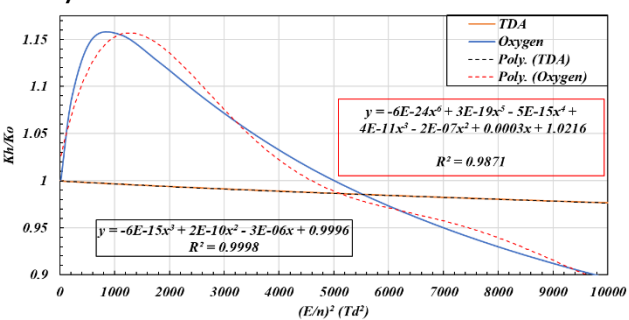


Figure 4.  $K_h/K_0 vs. (E/n)^2$  for oxygen and TDA ions. TDA can be approximated using a third-degree (sixth for E/n) polynomial accurately. However, the curve for oxygen cannot be easily represented. To generate this figure, the mobility of oxygen was taken from ref<sup>42</sup>, whereas the mobility of TDA is calculated using data from this work.

In order to fully take advantage of the combined DMA-FAIMS data, it is necessary to transform the dispersion plot into a mobility versus field plot. This can be done through the Buryakov equation, or, in some cases, a more generally valid expression as shown below. The field dependent mobility  $K_h(E)$  can be expressed as:

$$K_h(E) = K_0(1 + \alpha_E), \tag{2}$$

where  $K_0$  is the zero-field mobility and  $\alpha_E$  is a function that accounts for the high-field effects.  $\alpha_E$  is generally expressed as a series of even powers of the reduced field strength (E/n):

$$\alpha_E = \sum_{p=1}^{\infty} \alpha_{2p} (E/n)^{2p}. \tag{3}$$

Here the  $\alpha_{2p}$  coefficients are assumed to be independent of the field, i.e., constant. The vertical velocity equation  $\langle V_c \rangle = 0$  can be expanded using eq. (2) to provide the necessary compensation field required for optimum ion transmission<sup>14, 43, 44</sup>:

$$E_c = \frac{\sum_{p=1}^{\infty} \alpha_{2p} E_s^{2p+1} \langle f^{2p+1} \rangle}{1 + \sum_{p=1}^{\infty} (2p+1) \alpha_{2p} E_s^{2p} \langle f^{2p} \rangle}.$$
 (4)

Eq. (4) is specifically the Buryakov equation and, while valid for smooth varying functions, it turns out that it will lead to significant errors for complex functions. This is showcased in Figure 4 where the relative mobility is given as a function of the reduced field strength for TDA+ and  $O^+$ . For  $TDA^+$ , the  $\alpha_E$  parameter to be used in eq. (3) can be obtained by an interpolating polynomial rather easily. However, for  $O^+$ , no interpolating polynomial with constant coefficients can accurately follow the curve properly, leading to an error when trying to calculate  $E_c$ . In general, for a type-C ion (see figure 2), it may be a simple task, but for a type-B or type-D ion<sup>21, 45</sup>, it might not be possible. Type-D ions have recently appeared in literature to represent different behaviors which are uncommon and unrelated to the other three types. More specifically, *TDA*<sup>+</sup> can be represented using only a third-degree polynomial, however  $0^+$  cannot be represented even by a  $6^{th}$  degree polynomial as shown in figure 4. This complication can perhaps be circumvented by breaking the curve into multiple parts as theorized by 46, 47; however, this still requires polynomials to be formed and might not always be suitable. The reason stems from the fact, as shown below by the two-temperature theory (2TT), that the  $\alpha_{2m}$  coefficients are not necessarily constants but instead are intricate ratios of series of even powers of the field. As such, a simple polynomial might be insufficient. Since eq. (3) is used to arrive at eq. (4), then eq. (4) is no longer generally valid. The issue can be fixed by assuming that  $\alpha(E) = \alpha_E$ is instead a more general even function of the field. Starting again from  $\langle V_c \rangle = \langle K(E) \cdot E(t) \rangle = 0$  and using eq. (2) one can write:

$$K_0\langle (1+\alpha_E) (E_s(t)+E_c)\rangle = 0.$$

Since  $K_0$  is a non-zero constant independent of the field, the equation can be expanded as,

$$\langle E_s(t) \rangle + \langle E_c \rangle + \langle \alpha_E E_s(t) \rangle + \langle \alpha_E E_c \rangle = 0.$$

Moreover, since  $\langle E_c \rangle = E_c$  and  $\langle E_s(t) \rangle = 0$  (requirement of DMS), the equation is now,

$$E_c = -\frac{\langle \alpha_E E_s(t) \rangle}{1 + \langle \alpha_E \rangle} \tag{5}$$

Eq. (5) is an implicit equation that needs to be solved iteratively since  $\alpha_E$  is a function of  $E_c$  and  $E_s(t)$  both. Schneider et al. proposed that a Taylor expansion of the numerator around small values of the compensation voltage could be used and only the first few terms kept<sup>48</sup>. However, errors would be expected when high compensation voltages would be used. Haack et al. initially adopted this procedure<sup>28</sup> but have very recently proposed an iterative approach that calculates the displacement of the ions directly through compensation voltage guesses and corrections<sup>29</sup>. Our approach to solving eq. (5) is less compu-

tationally involved.  $\langle \alpha_E \rangle$  and  $\langle \alpha_E E_s(t) \rangle$  are calculated using a stepwise integration method by creating a spline from discrete nodes mathematically. In this way, Eq. (5) can be used indifferently to obtain an  $E_s-E_c$  dispersion plot or a  $K_h/K_0-E/n$  mobility plot depending on the data provided accurately. In the case of the smooth varying TAA salts, either eq. (4) or (5) may be employed using the experimental data.

In order to theoretically infer the mobility as a function of the field from all-atom models to compare it to the results of the DMA/FAIMS, the one-temperature theory Mason-Schamp equation<sup>7, 8</sup> may not be used, unfortunately, as it cannot capture the field-dependent behavior. To achieve this goal, different theories such as the twotemperature theory (2TT)<sup>8, 49</sup>, the three-temperature theory (3TT)50-52, Gram-Charlier53, 54 theory, among others have been developed. Recent developments in the 2TT have showcased that it can be used on polyatomic ions quite successfully23, 28 and software enabling up to the fourth order approximation is now available<sup>21</sup>. The 2TT has been thoroughly explained elsewhere and will only be briefly discussed here<sup>24, 28, 55-57</sup>. As its name suggests, in the 2TT the temperature of the ion can deviate from the temperature of the gas in order to accommodate the energy received from the field and from collisions with the gas. In general, the 2TT mobility equation of  $k^{th}$  order  $(K_{h_k})$ can be written as:

$$K_{h_{k}}(E) = \frac{3}{16} \frac{qe}{n} \left( \frac{2\pi}{\mu k T_{eff}} \right)^{\frac{1}{2}} \frac{1}{\Omega_{T_{eff}}^{(1,1)}} \left( 1 + \sum_{p=1}^{k-1} \beta_{p} \left( \frac{E}{n} \right)^{2p} \right) = K_{h_{l}} \left( 1 + \sum_{p=1}^{k-1} \beta_{p} \left( \frac{E}{n} \right)^{2p} \right)$$

$$(6)$$

Here qe, is the ion's charge,  $\mu$  is the reduced mass, k is the Boltzmann constant,  $T_{eff}$  is the effective temperature of the ion which accounts for the ion heating and  $\bar{\Omega}_{T_{eff}}^{(1,1)}$  is the collision cross section (CCS) calculated at  $T_{eff}$ .  $T_{eff}$  is obtained theoretically by calculating the energy moment of the Boltzmann equation and as a first approximation can be given by the Wannier eq.  $T_{eff} = T_0 + mv_d^2/3k$ , with M the mass of the ion. The  $\beta_p$  coefficients are intricate functions of collision integrals  $\bar{\Omega}_{T_{eff}}^{(l,s)}$ , and  $K_{h_I}$  is the first approximation of the ion mobility at an arbitrary field.  $K_{h_I}$ , unlike  $K_0$ , is not a constant value for different fields. In fact, the relation between  $K_{h_I}$  and  $K_0$  is given by (using 1TT Mason-Schamp eq. and eq. (6)):

$$K_{h_I} = K_0 \left(\frac{T_0}{T_{eff}}\right)^{1/2} \frac{\bar{\Omega}_{T_0}^{(1,1)}}{\bar{\Omega}_{T_{eff}}^{(1,1)}},\tag{7}$$

where  $T_0$  is the bath gas temperature.  $T_0$  and  $T_{eff}$ , and thus  $K_{h_I}$  and  $K_0$ , coincide at the zero field. By looking at eq. (2), it can be reasoned that as a first approximation:

$$\left(\frac{T_0}{T_{eff}}\right)^{1/2} \frac{\bar{\Omega}_{T_0}^{(1,1)}}{\bar{\Omega}_{T_{eff}}^{(1,1)}} = (1 + \alpha_E) = \left(1 + \sum_{p=1}^{\infty} \alpha_{2p} \left(\frac{E}{n}\right)^{2p}\right), \quad (8)$$

while the term  $(1 + \sum_{p=1}^{k-1} \beta_p (E/n)^{2p})$  can be added to eq. (8) for higher approximations. Since  $T_{eff} = T_0 + m(KE)^2/3k$  is a complicated function of the field (although still an even function), it is therefore reasonable to expect that the  $\alpha_{2p}$  coefficients are also complex functions of the field and not constant.

The Ion Mobility Software Suite (IMoS v.1.12) was used to calculate the mobility at arbitrary fields, with a fourthorder approximation of the 2TT<sup>21, 22</sup>. The results from the simulations can be compared to the experimental ones by either transforming the experimental dispersion plot into a mobility-field plot or vice versa. Here we have opted for the former. We then compare extracted mobility curves versus field strength to predictions using the twotemperature theory approach. A priori, we expect the theory will fail at higher field strengths due to the inelasticity of ion-gas molecule collisions and a hitherto unknown inelasticity term must be added to the calculations to match the experimental results. The deviation at high fields, in particular for polyatomic gases was predicted and experimentally observed by Ellis et al.42, 58, while the work by Siems et al. discusses the effect of high-field and possible deviations in detail<sup>25</sup>. Krylov et al. created a fitting procedure for their experimental data based on an energy loss ratio59. More recent experimental work by Schaefer et al. focuses on high-field energy corrections using the Hike-IMS<sup>27</sup>.

# Inferring Field-Dependent Mobilities from data

With the information obtained through the dispersion curve, one could calculate the mobility at a non-negligible electric field by calculating the  $\alpha$  coefficients. To do so, eq. (4) may be expanded for m=3 which results in:

$$-E_c = c_3 E_D^3 + c_5 E_D^5 + c_7 E_D^7, (9)$$

where  $c_3 = \alpha_2 \langle f^3 \rangle$ ,  $c_5 = \alpha_4 \langle f^5 \rangle - 3c_3\alpha_2 \langle f^2 \rangle$ , and  $c_7 = \alpha_6 \langle f^7 \rangle - 3c_5\alpha_2 \langle f^2 \rangle - 5c_3\alpha_4 \langle f^4 \rangle$ . The equation can be further simplified to  $y = c_3 + c_5 x + c_5 x^2$  where  $y = -E_c/E_D^3$ and  $x = E_D^2$ . For a bisinusoidal wave,  $\langle f^2 \rangle = 0.2777$ ,  $\langle f^3 \rangle = 0.1111, \quad \langle f^4 \rangle = 0.1527 \quad \langle f^5 \rangle = 0.1132, \quad \langle f^7 \rangle = 0.1132$ 0.1020 were obtained numerically. Table 1 displays the values of  $\alpha_2$ ,  $\alpha_4$ , and  $\alpha_6$ , which were calculated through a polynomial regression using the centerline data points provided in table S.1 for the different cations. In order to represent the results, the zero-field mobility is obtained using the results from the simulations rather than the results from the DMA (1.38 cm<sup>2</sup>/Vs, 0.955 cm<sup>2</sup>/Vs, 0.78 cm<sup>2</sup>/Vs and, 0.72 cm<sup>2</sup>/Vs respectively, with a 1% difference on average with respect to experimental results), with the reasoning that the FAIMS total mobility values at high field can be better compared to simulations this way. The visual representation of the mobility as a function of E/nis shown in Figure 5 confirming that the mobility of TAA ions decreases as the field is increased. In this sense, dispersion plots can provide experimental mobility at high field48,60 and can easily be compared to theory. Using eq. (5) instead of (4) would have led to similar results given the smooth variation of mobility of the salts.

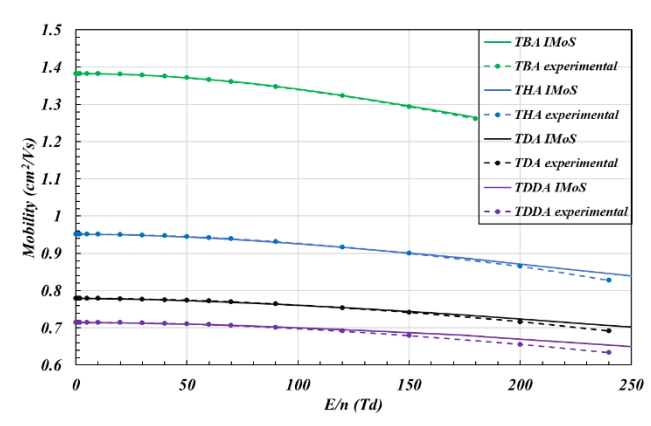
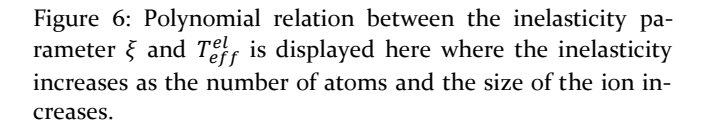


Figure 5. Comparison of experimental and simulated mobility at non-negligible field-over-gas concentration (E/n). Experimental and simulated mobilities are in very good agreement until 100Td after which, the difference is increased systematically due to inelastic collisions.

Table 1. Estimated  $\alpha_{2p}$  values using the centreline data and equation 9. In units of  $(1/Td)^{2p}$ .

	TBA	THA	TDA	TDDA
$\alpha_2$	-3.3751E-06	-2.7307E-06	-2.4929E-06	-2.4845E- 06
$\alpha_4$	2.8043E-11	1.9201E-11	1.8229E-11	1.4072E-11
$\alpha_6$	-2.4705E-16	-1.8659E-16	-1.5439E-16	-8.9699E-17

The 2TT 4th approximation to the mobility was calculated using the 4-6-12 LJTM method and using the default LJ parameters for diatomic nitrogen. The results for K vs E/n are given in figure 5 and they are compared against the experimental results. The structures were obtained using Density Functional Theory and optimized at 0 Td using Gaussian v.1661. To obtain the optimized structures, an initial geometry was created in Avogadro<sup>62</sup> using Molecular Mechanics (MM2) calculations. Then the geometry was optimized using the B<sub>3</sub>LYP<sup>63-66</sup> functional, and 6-31G(d,p)<sup>67</sup> Pople basis. The simulated results show very good agreement with experiments up to at least 100 Td. However, past 100 Td, the calculation results begin to systematically deviate from the experimental measurements, with differences more apparent as the field is increased. It is therefore expected that there are alternative effects that have not been considered yet in model calculations. One of the possibilities is that the ions become larger as the effective temperature is increased. Since THA+, TDA+, and TDDA+ are rather flexible ions<sup>68</sup>, this cannot be ruled out for them. In fact, relaxation effects between low and high field phases could also be important but its impact is something difficult to characterize at present. A second possibility is that inelastic collisions in diatomic gases have been known to exist that will affect the mobility. Regarding the latter, Wilks and co-workers have previously observed a similar trend and proposed to use a constant collision efficiency (or inelasticity coefficient) value to accurately predict the dispersion curve accurately<sup>69</sup>. A closer look at the assumptions used to derive the two-temperature theory reveals that it assumes elastic collisions, throwing further light on the problem. In fact, Viehland hypothesized and experimentally endorsed that upon a collision, the ion might transfer some of its kinetic energy to the internal energy of the gas molecule <sup>70, 71</sup>. While this phenomenon might be unimportant for monoatomic gases like helium, it may have a more considerable impact in polyatomic gases <sup>72</sup>.



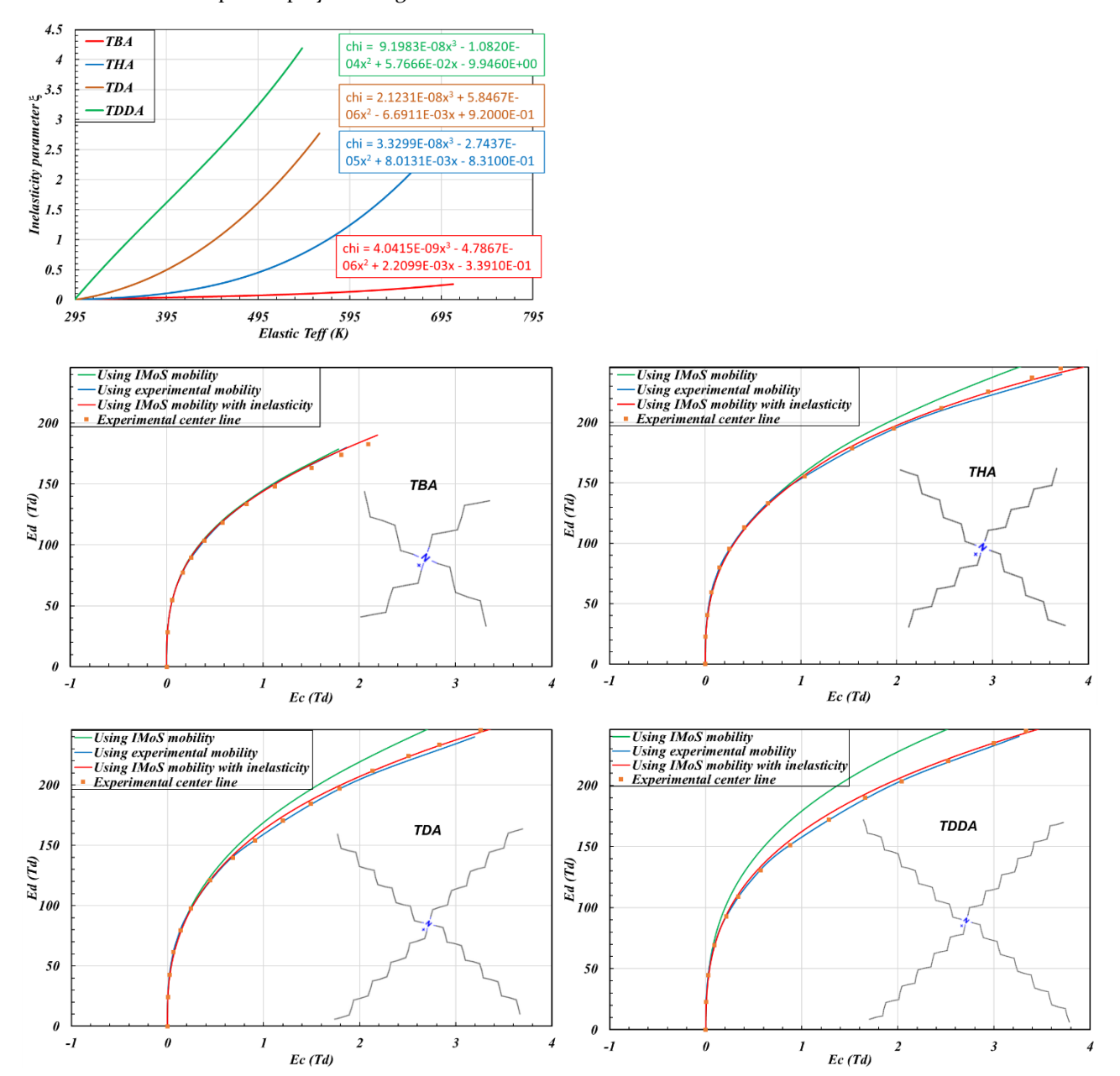


Figure 7. Dispersion curve of TBA, THA, TDA, and TDDA is presented. The points at which the experimental data was collected are represented by orange squares. Using the experimental data,  $\alpha$  coefficients were calculated which were then used to calculate mobility at high field. This mobility was then used in equation 5 to create the blue line. The overlapping of blue line and orange squares suggests that the equation 5 is suitable for predicting the dispersion curve. The red line was created by including an inelasticity parameter in calculation of mobility vs E/n curve.

At this point, it is not easy to differentiate whether the effect comes from the enlargement of the structures or from inelasticity, or both. While inelasticity can technically be calculated theoretically using the Wang Chang-Uhlenbeck-de Boer (WUB) equation, it is much too complex to be used for polyatomic ions and not attempted here. We believe it suffices for the time being that inelas-

ticity may be calculated experimentally through the equation 71:

$$\frac{3}{2}kT_{eff}^{inel}\left(1+\frac{m}{M}\xi\right) = \frac{3}{2}kT_{eff}^{el},\tag{10}$$

where  $T_{eff}^{inel}$  represents the inelastic experimental or WUB effective temperature and  $T_{eff}^{el}$  represents the elastic or 2TT effective temperature that is calculated through the

simulation. The ratio m/M is the ratio of the mass of the gas to the mass of the ion.

One can make use of eq. (10) and the mobility results to calculate the value of  $\xi$  by associating the values of  $T_{eff}$  at a given mobility. The obtained value of  $\xi$  might contain a part of the deviation that arises from the partial unfolding of the structures. A regression fit between  $\xi$  and  $T_{eff}^{el}$  was obtained and is illustrated in figure 6. Using this relation,  $(E/n)_{el}^{2TT}$  was converted to  $(E/n)_{inel}^{2TT}$ . The accuracy of this relation can be demonstrated in the  $K_h vs E/n$  curve, however, it is more convenient to present the results using dispersion plots. As such, eq. (5) is used to calculate the dispersion plots from the uncorrected as well as the inelasticity-corrected simulation results and compared to experiments as shown in figure 7 for all four salts (figure S.3 shows the results in the mobility-E/n domain). Figure 7 also shows both the center line values from the experimental data of figure S.2 as well as the transformation of the experimental mobility calculated in figure 5 using the polynomial interpolation. The new relationship between the simulations and the experimental center line after the inelastic/unfolding correction resulted in an average difference between theory and experiments of 1.5551%, 0.8271%, 1.1944%, and 1.6328% for TBA, THA, TDA, and TDDA, respectively. It can be observed that as the size of the salt increases, the effect of  $\xi$  is stronger, which can be attributed to both mobility-reducing mechanisms. However, for the smallest salt, TBA, simulations suggest little unfolding and therefore most of the effect from  $\xi$  can be attributed in this case to inelasticity. And, in all cases, it can be observed that the effect is only important at high fields (> 100Td). The inelasticity values obtained here are much larger than those obtained by Schaeffer et al.27 but of the same order of magnitude as those of Ellis et al<sup>42, 49</sup>. Finally, other inelasticity effects could be present even for atomic ions in atomic gases which have been studied by Siems' et al<sup>26</sup>. While there is clearly an effect, further investigation is indeed necessary to fully understand the underlying mechanism. In particular, given the clear evidence that a mobility reducing effect is present, the use of more rigid structures can now be used to try and determine the direct effect of inelasticity.

# **Conclusions**

This work deals with the study of a combination of a half-mini-DMA and a FAIMS system to improve ion filtration and provide simultaneous low-field and variable field mobility data on ions. Because both the DMA and FAIMS are band pass filters, instrument coupling is simpler than a FAIMS with a drift tube ion mobility spectrometer (DTIMS), where either a gating procedure needs to be developed with the DTIMS upstream, or the FAIMS needs to be electrically floated above the drift tube (or modified drift tube operation is required, e.g. frequency domain DTIMS<sup>73</sup>). The ions separated via DMA-FAIMS can be identified with a higher level of confidence since the two devices employ distinct concepts of ion mobility to separate ions. The resulting mobility spectra results can then be used to investigate whether the two-temperature theory (2TT) may be used for polyatomic ions at arbitrary

fields in diatomic gases. Since the raw data provided by the FAIMS is a dispersion plot, an equation is needed that relates the compensation and separation fields to the ion mobility at arbitrary fields. While the Buryakov equation has been used for this purpose in the past, it is shown in this work that it is not universal, and a more general equation is provided. With this equation, the comparison between the 2TT and experimental mobility is made with very satisfactory results. The results match within 1% up to 100Td, after which the experimental results deviate from theory. This is attributed to two effects, a) unfolding of the larger cations due to an increase in the effective temperature and b) inelasticity of the gas-ion collisions due to the higher effective temperature of the ion and the diatomic nature of the gas. By using the WUB theory, experiments and theory are matched through the use of the inelastic parameter  $\xi$ . The inelasticity is shown to be larger with larger salts, but caution about its absolute value is advised as the effect of unfolding on the salts needs to be properly accounted for. This study however validates the 2TT in nitrogen up to reasonable values of the field for the first time.

#### **ASSOCIATED CONTENT**

#### **Supporting Information**

Experimental mobility spectra of cations and cluster ions; experimental dispersion curve and its center line data; experimental and simulated mobility comparison; co-ordinates and partial charges of atoms in the optimized structures of ions are provided in the supplementary material file named: "FAIMS and inelasticity in N2\_SI.docx". The Supporting Information is available free of charge on the ACS Publications website.

#### **AUTHOR INFORMATION**

#### Corresponding Author

Carlos Larriba-Andaluz: <u>clarriba@iupui.edu</u> Christopher J. Hogan: <u>hoganio8@umn.edu</u>

# **Present Addresses**

†J.L. is now affiliated with Seagate Technology, Bloomington, MN, 55435

## **Author Contributions**

V.D.G. and J.L. contributed equally. The manuscript was written through contributions of all authors.

# Notes

The authors declare no competing financial interest.

#### **ACKNOWLEDGMENT**

C.L.A. acknowledges the financial support provided by NSF Division of Chemistry under Grant No. 1904879 and No. 2203968 and C.J.H. acknowledges the financial support provided by NSF award 2002852.

<u>Insert Table of Contents artwork here [after ref]</u>

Graphical abstract: 3.25 in by 1.75 in

#### **REFERENCES**

- (1) Andrzejewski, R.; Entwistle, A.; Giles, R.; Shvartsburg, A. A. Ion Mobility Spectrometry of Superheated Macromolecules at Electric Fields up to 500 Td. *Analytical Chemistry* **2021**, *93* (35), 12049-12058.
- (2) Gandhi, V. D.; Larriba-Andaluz, C. Predicting ion mobility as a function of the electric field for small ions in light gases. *Analytica Chimica Acta* **2021**, *1184*, 339019.
- (3) Harrilal, C. P.; Gandhi, V. D.; Nagy, G.; Chen, X.; Buchanan, M. G.; Wojcik, R.; Conant, C. R.; Donor, M. T.; Ibrahim, Y. M.; Garimella, S. V. Measurement and Theory of Gas-Phase Ion Mobility Shifts Resulting from Isotopomer Mass Distribution Changes. *Analytical Chemistry* 2021, 93 (45), 14966-14975.
- (4) Hornbeck, J. A. The drift velocities of molecular and atomic ions in helium, neon, and argon. *Physical Review* **1951**, *84* (4), 615.
- (5) Hornbeck, J. A. The mobilities of molecular and atomic rare gas ions in the parent gases: helium, neon, and argon. *Physical Review* **1950**, *80* (2), 297.
- (6) Chen, X.; Gandhi, V.; Coots, J.; Fan, Y.; Xu, L.; Fukushima, N.; Larriba-Andaluz, C. High resolution varying field drift tube ion mobility spectrometer with diffusion autocorrection. *Journal of Aerosol Science* **2020**, *140*, 105485.
- (7) Mason, E. A.; Schamp Jr, H. W. Mobility of gaseous lons in weak electric fields. *Annals of physics* **1958**, *4* (3), 233-270.
- (8) Viehland, L. A.; Mason, E. Gaseous lon mobility in electric fields of arbitrary strength. *Annals of Physics* **1975**, *91* (2), 499-533.
- (9) Jin, W.; Jarvis, M.; Star-Weinstock, M.; Altemus, M. A sensitive and selective LC-differential mobility-mass spectrometric analysis of allopregnanolone and pregnanolone in human plasma. *Analytical and bioanalytical chemistry* 2013, 405 (29), 9497-9508.
- (10) Cohen, A.; Ross, N. W.; Smith, P. M.; Fawcett, J. P. Analysis of 17β-estradiol, estriol and estrone in American eel (Anguilla rostrata) tissue samples using liquid chromatography coupled to electrospray differential ion mobility tandem mass spectrometry. *Rapid Communications in Mass Spectrometry* **2017**, 31 (10), 842-850.
- (11) Rus, J.; Moro, D.; Sillero, J. A.; Royuela, J.; Casado, A.; Estevez-Molinero, F.; de la Mora, J. F. IMS–MS studies based on coupling a differential mobility analyzer (DMA) to commercial API–MS systems. *International Journal of Mass Spectrometry* 2010, 298 (1-3), 30-40.
- (12) Knutson, E. O.; Whitby, K. T. Aerosol classification by electric mobility: apparatus, theory, and applications. *Journal of Aerosol Science* **1975**, *6* (6), 443-451. DOI: <a href="http://dx.doi.org/10.1016/0021-8502(75)90060-9">http://dx.doi.org/10.1016/0021-8502(75)90060-9</a>.
- (13) Rus, J.; Moro, D.; Sillero, J. A.; Royuela, J.; Casado, A.; Estevez-Molinero, F.; de la Mora, J. F. IMS-MS studies based on coupling a differential mobility analyzer (DMA) to commercial API-MS systems. *International Journal of Mass Spectrometry* 2010, 298 (1-3), 30-40.
- (14) Buryakov, I.; Krylov, E.; Nazarov, E.; Rasulev, U. K. A new method of separation of multi-atomic ions by mobility at atmospheric pressure using a high-frequency amplitude-asymmetric strong electric field. *International*

- Journal of Mass Spectrometry and Ion Processes 1993, 128 (3), 143-148.
- (15) Safaei, Z.; Eiceman, G. A.; Puton, J.; Stone, J. A.; Nasirikheirabadi, M.; Anttalainen, O.; Sillanpaa, M. Differential Mobility Spectrometry of Ketones in Air at Extreme Levels of Moisture. *Sci Rep* **2019**, *9* (1), 5593. DOI: 10.1038/s41598-019-41485-7.
- (16) Kolakowski, B. M.; Mester, Z. Review of applications of high-field asymmetric waveform ion mobility spectrometry (FAIMS) and differential mobility spectrometry (DMS). *Analyst* **2007**, *132* (9), 842-864.
- (17) Shvartsburg, A. A.; Mashkevich, S. V.; Smith, R. D. Feasibility of higher-order differential ion mobility separations using new asymmetric waveforms. *The Journal of Physical Chemistry A* **2006**, *110* (8), 2663-2673.
- (18) Huxley, L. LXXV. The corona discharge in helium and neon. *The London, Edinburgh, and Dublin Philosophical Magazine and Journal of Science* **1928**, 5 (30), 721-737.
- (19) Mitchell, J.; Ridler, K. The speed of positive ions in nitrogen. *Proceedings of the Royal Society of London.* Series A, Containing Papers of a Mathematical and Physical Character **1934**, 146 (859), 911-921.
- (20) Tyndall, A. M. *The mobility of positive ions in gases*; Cambridge University Press.–1938.–Cambridge.-UK.
- (21) Gandhi, V. D.; Short, K.; Hua, L.; Rodríguez, I.; Larriba-Andaluz, C. A numerical tool to calculate ion mobility at arbitrary fields from all-atom models. *Journal of Aerosol Science* **2022**, 106122.
- (22) Shrivastav, V.; Nahin, M.; Hogan, C. J.; Larriba-Andaluz, C. Benchmark Comparison for a Multi-Processing Ion Mobility Calculator in the Free Molecular Regime. *J Am Soc Mass Spectrom* **2017**, *28* (8), 1540-1551. DOI: 10.1007/s13361-017-1661-8.
- (23) Gandhi, V. D.; Larriba-Andaluz, C. Predicting ion mobility as a function of the electric field for small ions in light gases. *Analytica Chimica Acta* **2021**, 339019.
- (24) Gandhi, V. D.; Hua, L.; Chen, X.; Latif, M.; Larriba-Andaluz, C. A critical review of the two-temperature theory and the derivation of matrix elements. High field ion mobility and energy calculation for all-atom structures in light gases using a 12-6-4 potential. *Talanta Open* **2023**, 7, 100191. DOI: https://doi.org/10.1016/j.talo.2023.100191.
- (25) Siems, W. F.; Viehland, L. A.; Hill Jr, H. H. Improved momentum-transfer theory for ion mobility. 1. Derivation of the fundamental equation. *Analytical chemistry* **2012**, *84* (22), 9782-9791.
- (26) Siems, W. F.; Viehland, L. A.; Hill, H. H. Correcting the fundamental ion mobility equation for field effects. *Analyst* **2016**, *141* (23), 6396-6407, 10.1039/C6AN01353H. DOI: 10.1039/C6AN01353H.
- (27) Schaefer, C.; Kirk, A. T.; Allers, M.; Zimmermann, S. Ion mobility shift of isotopologues in a high kinetic energy ion mobility spectrometer (HiKE-IMS) at elevated effective temperatures. *Journal of the American Society for Mass Spectrometry* **2020**, *31* (10), 2093-2101.
- (28) Haack, A.; Bissonnette, J. R.; Ieritano, C.; Hopkins, W. S. Improved First-Principles Model of Differential Mobility Using Higher Order Two-Temperature Theory.

- Journal of the American Society for Mass Spectrometry **2022**, *33* (3), 535-547. DOI: 10.1021/jasms.1c00354.
- (29) Haack, A.; Hopkins, W. S. Kinetics in DMS: Modeling Clustering and Declustering Reactions. *Journal of the American Society for Mass Spectrometry* **2022**, *33* (12), 2250-2262. DOI: 10.1021/jasms.2c00224.
- (30) Gandhi, V. D.; Short, K.; Hua, L.; Rodríguez, I.; Larriba-Andaluz, C. A numerical tool to calculate ion mobility at arbitrary fields from all-atom models. *Journal of Aerosol Science* **2023**, *169*, 106122. DOI: <a href="https://doi.org/10.1016/j.jaerosci.2022.106122">https://doi.org/10.1016/j.jaerosci.2022.106122</a>.
- (31) Fernández de la Mora, J.; Kozlowski, J. Hand-held differential mobility analyzers of high resolution for 1–30nm particles: Design and fabrication considerations. *Journal of Aerosol Science* **2013**, *57*, 45-53. DOI: <a href="https://doi.org/10.1016/j.jaerosci.2012.10.009">https://doi.org/10.1016/j.jaerosci.2012.10.009</a>.
- (32) Fenn, J. B.; Mann, M.; Meng, C. K.; Wong, S. F.; Whitehouse, C. M. Electrospray ionization for mass spectrometry of large biomolecules. *Science* **1989**, *246* (4926), 64-71.
- (33) Hogan Jr, C. J.; De La Mora, J. F. Ion mobility measurements of nondenatured 12–150 kDa proteins and protein multimers by tandem differential mobility analysis–mass spectrometry (DMA-MS). *Journal of the American Society for Mass Spectrometry* **2011**, 22 (1), 158-172.
- (34) de la Mora, J. F.; Kozlowski, J. Hand-held differential mobility analyzers of high resolution for 1–30 nm particles: Design and fabrication considerations. *Journal of Aerosol Science* **2013**, *57*, 45-53.
- (35) Ude, S.; De La Mora, J. F. Molecular monodisperse mobility and mass standards from electrosprays of tetraalkyl ammonium halides. *Journal of Aerosol Science* **2005**, *36* (10), 1224-1237.
- (36) Attoui, M.; de la Mora, J. F. Flow driven transmission of charged particles against an axial field in antistatic tubes at the sample outlet of a Differential Mobility Analyzer. *Journal of Aerosol Science* **2016**, *100*, 91-96. DOI: <a href="https://doi.org/10.1016/j.jaerosci.2016.06.002">https://doi.org/10.1016/j.jaerosci.2016.06.002</a>.
- (37) Purves, R. W.; Guevremont, R.; Day, S.; Pipich, C. W.; Matyjaszczyk, M. S. Mass spectrometric characterization of a high-field asymmetric waveform ion mobility spectrometer. *Review of Scientific Instruments* **1998**, *69* (12), 4094-4105.
- (38) Krylov, E. V.; Coy, S. L.; Vandermey, J.; Schneider, B. B.; Covey, T. R.; Nazarov, E. G. Selection and generation of waveforms for differential mobility spectrometry. *Review of Scientific Instruments* **2010**, *81* (2), 024101.
- (39) Aksenov, A. A.; Kapron, J.; Davis, C. E. Predicting compensation voltage for singly-charged ions in high-field asymmetric waveform ion mobility spectrometry (FAIMS). *Journal of the American Society for Mass Spectrometry* **2012**, *23* (10), 1794-1798.
- (40) Aksenov, A. A.; Kapron, J. T. Behaviour of tetraalkylammonium ions in high-field asymmetric waveform ion mobility spectrometry. Rapid Communications in Mass Spectrometry: An International Journal Devoted to the Rapid Dissemination of Up-to-the-Minute Research in Mass Spectrometry 2010, 24 (10), 1392-1396.

- (41) Campbell, J. L.; Zhu, M.; Hopkins, W. S. Ionmolecule clustering in differential mobility spectrometry: lessons learned from tetraalkylammonium cations and their isomers. *Journal of the American Society for Mass Spectrometry* **2014**, *25* (9), 1583-1591.
- (42) Ellis, H.; Pai, R.; McDaniel, E.; Mason, E.; Viehland, L. Transport properties of gaseous ions over a wide energy range. *Atomic Data and Nuclear Data Tables* **1976**, *17* (3), 177-210.
- (43) Buryakov, I. Mathematical analysis of ion motion in a gas subjected to an alternating-sign periodic asymmetric-waveform electric field. *Technical physics* **2006**, *51* (9), 1121-1126.
- (44) Lee, J. Aerosol Ion Mobility based Techniques for the Improved Analysis of Chemical Mixtures. University of Minnesota, 2021, 2021.
- (45) Crouse, J.; Haack, A.; Benter, T.; Hopkins, W. S. Understanding Nontraditional Differential Mobility Behavior: A Case Study of the Tricarbastannatrane Cation, N(CH2CH2CH2)3Sn+. *Journal of the American Society for Mass Spectrometry* **2020**, *31* (4), 796-802. DOI: 10.1021/jasms.9b00042.
- (46) Shvartsburg, A. A.; Smith, R. D.; Wilks, A.; Koehl, A.; Ruiz-Alonso, D.; Boyle, B. Ultrafast Differential Ion Mobility Spectrometry at Extreme Electric Fields in Multichannel Microchips. 2009. DOI: doi.org/10.1021/ac900892u.
- (47) Shvartsburg, A. A. Differential ion mobility spectrometry: nonlinear ion transport and fundamentals of FAIMS; CRC Press, 2008.
- (48) Schneider, B. B.; Nazarov, E. G.; Londry, F.; Vouros, P.; Covey, T. R. Differential mobility spectrometry/mass spectrometry history, theory, design optimization, simulations, and applications. *Mass Spectrometry Reviews* **2016**, *35* (6), 687-737.
- (49) Ellis, H.; McDaniel, E.; Albritton, D.; Viehland, L.; Lin, S.; Mason, E. Transport properties of gaseous ions over a wide energy range. Part II. *Atomic data and nuclear data tables* **1978**, *22* (3), 179-217.
- (50) Viehland, L. A.; Lin, S. Application of the three-temperatue theory of gaseous ion transport. *Chemical Physics* **1979**, *43* (1), 135-144.
- (51) Lin, S.; Viehland, L.; Mason, E. Three-temperature theory of gaseous ion transport. *Chemical Physics* **1979**, *37* (3), 411-424.
- (52) Waldman, M.; Mason, E. Generalized Einstein relations from a three-temperature theory of gaseous ion transport. *Chemical Physics* **1981**, *58* (1), 121-144.
- (53) Ong, P.; Li, M.-M. Monte Carlo simulation studies on the validity of the Gram-Charlier calculations of velocity distributions of Na+ swarm in neon gas. *Chemical physics* **1996**, *211* (1-3), 115-122.
- (54) Viehland, L. A. Velocity distribution functions and transport coefficients of atomic ions in atomic gases by a Gram—Charlier approach. *Chemical physics* **1994**, *179* (1), 71-92.
- (55) Almeida, P.; Benilov, M.; Naidis, G. Calculation of ion mobilities by means of the two-temperature displaced-distribution theory. *Journal of Physics D: Applied Physics* **2002**, *35* (13), 1577.

- (56) Larriba-Andaluz, C.; Prell, J. S. Fundamentals of ion mobility in the free molecular regime. Interlacing the past, present and future of ion mobility calculations. *International Reviews in Physical Chemistry* 2020, 39 (4), 569-623.
- (57) Viehland, L. A.; Mason, E. Gaseous ion mobility and diffusion in electric fields of arbitrary strength. *Annals of Physics* **1978**, *110* (2), 287-328.
- (58) Mason, E. A.; McDaniel, E. W. *Transport properties of ions in gases*; John Wiley & Sons., 1988. DOI: dx.doi.org/10.1002/3527602852.
- (59) Krylov, E. V.; Coy, S. L.; Nazarov, E. G. Temperature effects in differential mobility spectrometry. *International Journal of Mass Spectrometry* **2009**, *279* (2), 119-125. DOI: https://doi.org/10.1016/j.ijms.2008.10.025.
- (60) Krylov, E.; Nazarov, E.; Miller, R.; Tadjikov, B.; Eiceman, G. Field dependence of mobilities for gasphase-protonated monomers and proton-bound dimers of ketones by planar field asymmetric waveform ion mobility spectrometer (PFAIMS). *The Journal of Physical Chemistry A* **2002**, *106* (22), 5437-5444.
- (61) Gaussian 16 Rev. C.01; Wallingford, CT, 2016. (accessed.
- (62) Hanwell, M. D.; Curtis, D. E.; Lonie, D. C.; Vandermeersch, T.; Zurek, E.; Hutchison, G. R. Avogadro: an advanced semantic chemical editor, visualization, and analysis platform. *Journal of cheminformatics* 2012, 4 (1), 17.
- (63) Stephens, P. J.; Devlin, F. J.; Chabalowski, C. F.; Frisch, M. J. Ab initio calculation of vibrational absorption and circular dichroism spectra using density functional force fields. *The Journal of physical chemistry* **1994**, *98* (45), 11623-11627.
- (64) Becke, A. D. Becke's three parameter hybrid method using the LYP correlation functional. *J. Chem. Phys* **1993**, *98* (492), 5648-5652.
- (65) Lee, C.; Yang, W.; Parr, R. Density-functional exchange-energy approximation with correct asymptotic behaviour. *Phys. Rev. B* **1988**, *37*, 785-789.
- (66) Vosko, S. H.; Wilk, L.; Nusair, M. Accurate spindependent electron liquid correlation energies for local spin density calculations: a critical analysis. *Canadian Journal of physics* 1980, 58 (8), 1200-1211.
- (67) Dill, J. D.; Pople, J. A. Self-consistent molecular orbital methods. XV. Extended Gaussian-type basis sets for lithium, beryllium, and boron. *The Journal of Chemical Physics* **1975**, *62* (7), 2921-2923.
- (68) Merenbloom, S. I.; Flick, T. G.; Williams, E. R. How hot are your ions in TWAVE ion mobility spectrometry? *Journal of the American Society for Mass Spectrometry* **2011**, *23* (3), 553-562.
- (69) Wilks, A.; Hart, M.; Koehl, A.; Somerville, J.; Boyle, B.; Ruiz-Alonso, D. Characterization of a miniature, ultra-high-field, ion mobility spectrometer. *International Journal for Ion Mobility Spectrometry* 2012, 15 (3), 199-222.
- (70) Kaneko, Y.; Megill, L.; Hasted, J. Study of inelastic collisions by drifting ions. *The Journal of Chemical Physics* **1966**, *45* (10), 3741-3751.

- (71) Viehland, L.; Fahey, D. The mobilities of NO- 3, NO- 2, NO+, and Cl- in N2: A measure of inelastic energy loss. *The Journal of Chemical Physics* **1983**, 78 (1), 435-441.
- (72) Larriba-Andaluz, C. A perspective on the theoretical and numerical aspects of Ion Mobility Spectrometry. *International Journal of Mass Spectrometry* 2021, 470, 116719.
- (73) Morrison, K. A.; Siems, W. F.; Clowers, B. H. Augmenting Ion Trap Mass Spectrometers Using a Frequency Modulated Drift Tube Ion Mobility Spectrometer. *Analytical Chemistry* **2016**, *88* (6), 3121-3129. DOI: 10.1021/acs.analchem.5b04223.